Strategies for Landing Large Ballistic Coefficient Vehicles on Mars

Tyler R. Anderson*, Zachary R. Putnam†, and Robert D. Braun‡
Georgia Institute of Technology, Atlanta, Georgia, 30332

Large ballistic coefficient entry, descent, and landing vehicles are likely required to achieve more ambitious exploration goals at Mars. This paper investigates strategies for safe landing on Mars for vehicles with large ballistic coefficients, with a focus on maintaining sufficient altitude for terminal descent. Specifically, requirements and guidance strategies for the use of aerodynamic lift in the hypersonic regime are assessed over a range of ballistic coefficients. Results indicate that, for moderately high ballistic coefficients, judicious use of lift may allow safe landing. These strategies may be applicable to future large-scale robotic or human entry, descent, and landing architectures.

Nomenclature

$\mathbf{f}$	=	vector function
$\mathbf{p}$	=	co-state vector
$\mathbf{x}$	=	state vector
C_D	=	hypersonic drag coefficient
C_L	=	hypersonic lift coefficient
D	=	$\bar{q}S_{ref}C_D$, drag magnitude, N
$\bar{E}$	=	nondimensional trigger energy
EDL	=	Entry, Descent, and Landing
g	=	acceleration due to gravity, m/s^2
H	=	Hamiltonian
h	=	altitude, m
h_{floor}	=	energy trigger minimum altitude
h_{ref}	=	energy trigger reference altitude
H_{scale}	=	atmosphere scale height, m
J	=	cost function
L	=	$\bar{q}S_{ref}C_L$, lift magnitude, N
L/D	=	lift-to-drag ratio
m	=	mass, kg
MSL	=	Mars Science Laboratory
q	=	$\rho V^2/2$, dynamic pressure, N/m^2
R	=	planetary radius, m
S_{ref}	=	aerodynamic reference area, m^2
t	=	time, s
TDI	=	Terminal Descent Initiation
u	=	optimal control
V	=	velocity magnitude, m/s
V_{ref}	=	energy trigger reference velocity
β	=	$m/(C_D S_{ref})$, ballistic coefficient, kg/m^2
γ	=	flight-path angle, positive above local horizontal, rad

*Graduate Research Assistant, School of Aerospace Engineering, 270 Ferst Dr., Member AIAA.
†Research Engineer, School of Aerospace Engineering, 270 Ferst Dr., Senior Member AIAA.
‡Professor, School of Aerospace Engineering, 270 Ferst Dr., Fellow AIAA

λ = velocity-altitude scale factor
ρ = atmospheric density, kg/m^3
ρ_{ref} = atmosphere reference density, kg/m^3
σ = bank angle, rad
θ = range angle, rad

I. Introduction

Future Mars exploration mission goals will require landing more massive payloads at higher altitudes. The thin Martian atmosphere produces low drag forces on entry aeroshells, making it difficult decelerate sufficiently for terminal descent initiation prior to surface impact. Maximum diameter constraints imposed on aeroshells by launch vehicle fairings cause higher-mass vehicles to have larger ballistic coefficients, which reduces drag deceleration and makes safe landing of high-mass payloads more difficult. Achieving sufficient deceleration while retaining adequate timeline and altitude to execute terminal descent remains one of the primary challenges of landing vehicles on Mars.[1]

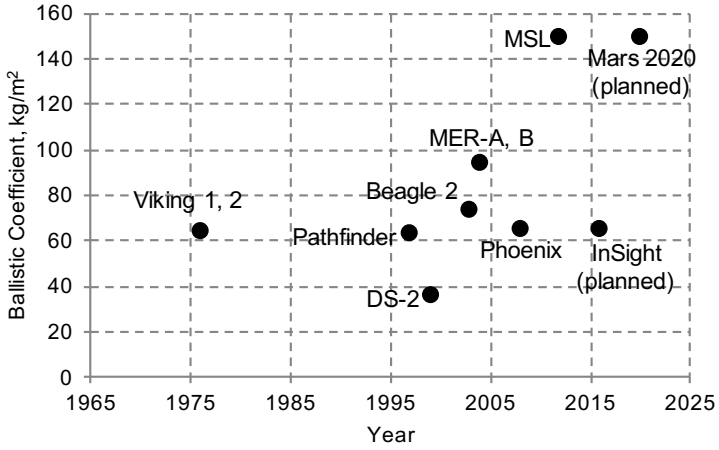

Figure 1. Ballistic coefficients of previous Mars landers.

Early Mars lander missions maintained relatively small ballistic coefficients near 60 kg/m^2 to ensure safe landing (see Fig. 1). Recently, more capable science platforms such as the 2012 Mars Science Laboratory (MSL) have nearly reached the ballistic coefficient limit for current Mars Entry, Descent, and Landing (EDL) technology. Fig. 2 shows the infeasibility of using supersonic parachutes as high ballistic coefficient vehicles drop below the parachute deploy region.[1] The 4.5 m diameter MSL aeroshell was near the allowable inner diameter for current 5 m launch vehicle fairings. MSL had a ballistic coefficient of approximately 145 kg/m^2 and landed a 1 t payload on the surface of Mars; this landed mass represents the current state of the art. Multiple technology options are being explored to mitigate this issue: lightweight deployable drag areas to reduce ballistic coefficient for higher-mass vehicles,[2,3] supersonic retropropulsion to improve deceleration during descent,[4] and high-performance parachutes to improve terminal descent margins.[3]

Figure 3 shows example entry trajectories at Mars for various ballistic coefficients and lift-to-drag ratios. The trajectories have a constant bank angle of zero; terminal descent initiation (TDI) occurs at 500 m/s. Fig. 3a shows that altitude at TDI decreases quickly with increasing ballistic coefficient. Vehicles with ballistic coefficients approaching 1000 kg/m^2 fail to reach 500 m/s prior to surface impact, even at the lowest possible surface elevations on Mars. Lift may be used to increase altitude at the terminal velocity state (see Fig. 3b). However, increased maximum lift-to-drag ratio does not necessarily guarantee improvement in altitude at TDI: flying a constant bank angle of zero at an L/D of 0.3 results in a lower altitude at 500 m/s than flight at $L/D = 0.2$. Lift must be applied intelligently over the trajectory to improve altitude at TDI. Lastly, the trajectories in Fig. 3 represent nominal conditions. Day-of-flight uncertainties in vehicle, environment, and state parameters significantly reduce expected attainable altitudes at 500 m/s. As examples

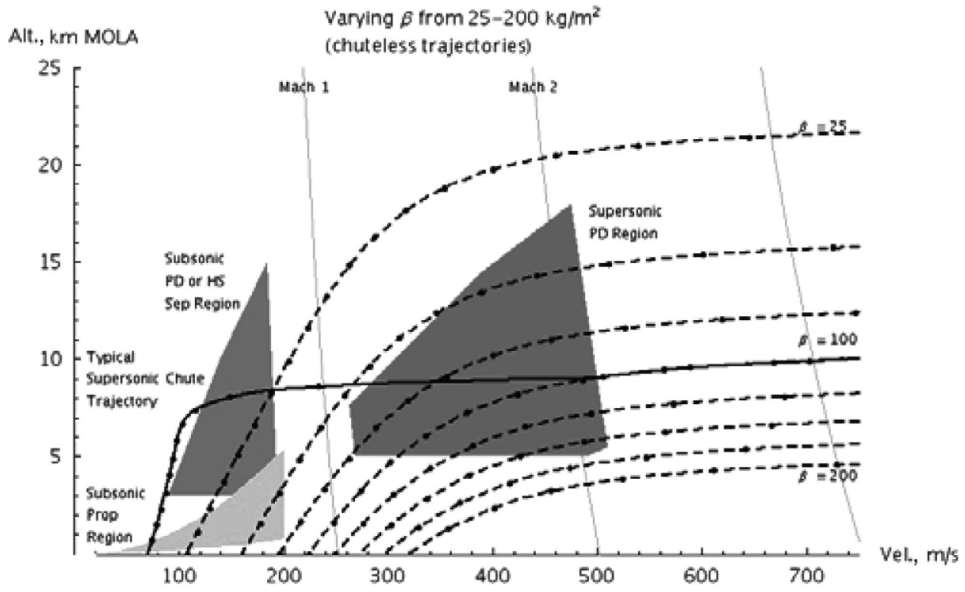

Figure 2. Parachute deploy regions with high β vehicles[1]

of large ballistic coefficient vehicles, a ballistic coefficient of 500 kg/m^2 corresponds roughly to a 60 t entry vehicle with a 10-m-diameter sphere-cone forebody or a 14 t vehicle with a 5-m-diameter forebody.

Previous strategies for maintaining sufficient altitude and timeline for terminal descent have focused on maintaining a lift-up or near-lift-up attitude during some portion of the entry. The use of lift for maintaining altitude was first studied in the 1960s. Depending on the mission requirements, lift can also be used to increase payload mass or reduce the loads at terminal descent initiation.[5] Later studies showed that a relatively small lift-to-drag ratio L/D was sufficient for near-term exploration goals.[6,7] Both Viking landers utilized a three-axis control system to maintain a 0 deg bank angle throughout entry. The Mars Science Laboratory flew range control with bank angle limited to $\pm$15 deg for velocities below 1100 m/s to maintain altitude prior to parachute deploy.[8]

This study investigates strategies for landing vehicles on Mars with ballistic coefficients significantly greater than current systems. The analyses presented focus on how best to maximize vehicle altitude and timeline margin at terminal descent initiation to ensure safe landing through use of lift in the hypersonic phase. These techniques may be applicable to future large-scale robotic or human EDL architectures.[9]

II. Maximum Altitude at Terminal Descent Initiation

The maximization of altitude for entry, descent, and landing trajectories at Mars is a well-known problem. Recent investigations include that of Lafleur and Cerimele, who attempted to determine optimal bank-command profiles for a notional high-mass, bank-to-steer lander.[10] Benito and Mease also used altitude maximization, recognizing it as a somewhat universal goal, as a way to reduce the dimensionality of reachable and controllable sets.[11] However, as shown by Garcia-Llama and others, optimal trajectories are often not robust to day-of-flight uncertainties in vehicle, environmental, and state parameters.[12] This study seeks to use optimal trajectory results to inform flight strategies, rather than dictate them, to achieve robust flight performance for high ballistic coefficient vehicles.

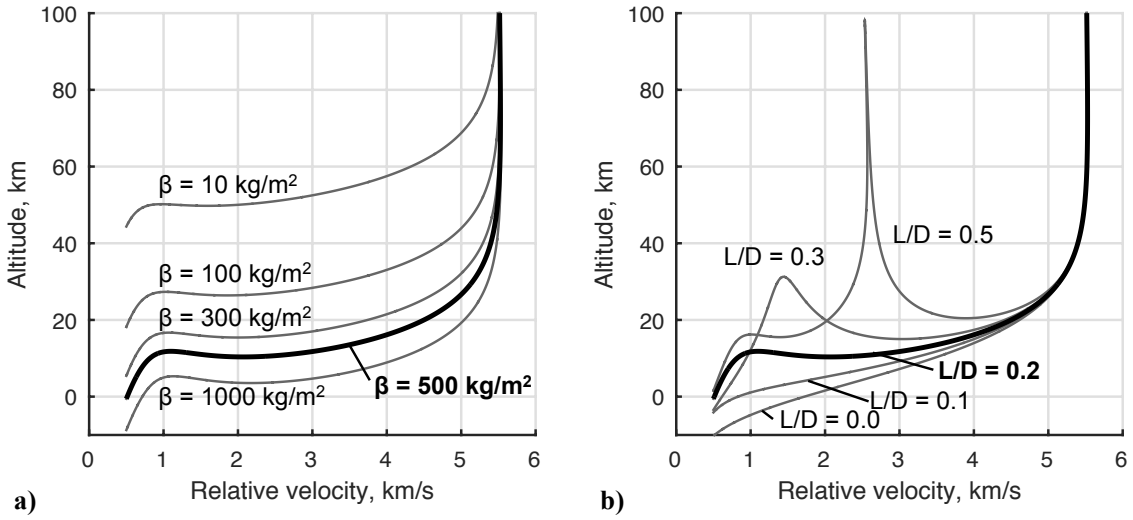

Figure 3. Entry trajectories for a) several ballistic coefficients with $L/D = 0.2$ and b) several L/D with $\beta = 500$ kg/m^2.

A. Altitude Maximization as an Optimal Control Problem

1. Problem Formulation

The planar equations of motion for a planetary entry vehicle may be written as:[13]

$$\dot{V} = -\frac{\rho V^2}{2\beta} - g\sin\gamma \tag{1a}$$

$$\dot{\gamma} = \frac{V\cos\gamma}{R+h} + \frac{\rho V}{2\beta}(L/D)\cos\sigma - \frac{g\cos\gamma}{V} \tag{1b}$$

$$\dot{h} = V\sin\gamma \tag{1c}$$

where the flight-path angle γ is defined to be positive above the local horizontal and $(L/D)\cos\sigma$ is the in-plane lift. Eq. (1) is a set of coupled, first-order, ordinary differential equations. These equations are highly nonlinear due to the presence of the planetary atmosphere and trigonometric functions and defy analytical solution unless simplifying assumptions are applied.

One can formulate the problem in terms of density instead of altitude, since altitude and density have a one-to-one relationship in the vast majority of applications. The cost function may be simply stated as a Mayer problem, or converted to a Lagrange problem:

$$J = -\rho_f = \int_{t_0}^{t_f} \left(\frac{\rho V}{H}\sin\gamma - \frac{\rho_0}{t_f - t_0} \right) dt \tag{2}$$

Neglecting h relative to R, converting from h to $-\rho$, and defining the optimal control as $u = \cos\sigma$:

$$\dot{\mathbf{x}} = \begin{bmatrix} \dot{V} \\ \dot{\gamma} \\ \dot{\rho} \end{bmatrix} = \begin{bmatrix} -\dfrac{\rho V^2}{2\beta} - g\sin\gamma \\ \dfrac{V\cos\gamma}{R} + \dfrac{\rho V}{2\beta}(L/D)u - \dfrac{g\cos\gamma}{V} \\ -\dfrac{\rho V\sin\gamma}{H} \end{bmatrix} = \mathbf{f}\left(t, \mathbf{x}, u\right) \tag{3}$$

The Hamiltonian is:

$$H = \mathbf{p}^T\mathbf{f}\left(t, \mathbf{x}, u\right) + \left(\frac{\rho V\sin\gamma}{H} - \frac{\rho_0}{t_f - t_0} \right) \tag{4}$$

Or:

$$H = p_V \left(-\frac{\rho V^2}{2\beta} - g \sin\gamma \right) + p_\gamma \left(\frac{V \cos\gamma}{R} + \frac{\rho V}{2\beta}(L/D)u - \frac{g \cos\gamma}{V} \right) - p_\rho \frac{\rho V \sin\gamma}{H} + \frac{\rho V \sin\gamma}{H} - \frac{\rho_0}{t_f - t_0} \quad (5)$$

By the Pontryagin minimum principle, the optimal control is:

$$u = \text{argmin}\left[H(u)\right] \quad (6)$$

Since H is a linear function of u and $u \in [-1, 1]$, the optimal control policy is "bang-bang" and the sign of u depends solely on the sign of the switching function:

$$f_s = p_\gamma \frac{\rho V}{2\beta}(L/D) \quad (7)$$

All of the quantities in the switching function are greater than zero, with the exception of the γ co-state, so the sign of the optimal control is dependent on the sign of p_γ. The values of the co-states are governed by:

$$\dot{p}_V = -\frac{\partial H}{\partial V} = p_V \frac{\rho V}{\beta} - p_\gamma \frac{\cos\gamma}{R} - p_\gamma \frac{\rho}{2\beta}(L/D)u - p_\gamma \frac{g}{V^2}\cos\gamma + \frac{\rho}{H}\sin\gamma\,(p_\rho - 1) \quad (8a)$$

$$\dot{p}_\gamma = -\frac{\partial H}{\partial \gamma} = p_V g \cos\gamma + p_\gamma \frac{V}{R}\sin\gamma - p_\gamma \frac{g}{V}\sin\gamma + \frac{\rho V}{H}\cos\gamma\,(p_\rho - 1) \quad (8b)$$

$$\dot{p}_\rho = -\frac{\partial H}{\partial \rho} = p_V \frac{V^2}{2\beta} - p_\gamma \frac{V}{2\beta}(L/D)u + \frac{V}{H}\sin\gamma\,(p_\rho - 1) \quad (8c)$$

Together, Eq. (3) and (8) form a two-point boundary-value problem with boundary conditions:

$$\begin{array}{cc} V(t_0) = V_0 & V(t_f) = V_f \\ \gamma(t_0) = \gamma_0 & p_\gamma(t_f) = 0 \\ \rho(t_0) = \rho_0 & p_\rho(t_f) = -1 \\ t_0 = 0 & H(t_f) = 0 \end{array} \quad (9)$$

2. Example Solution

To determine the structure of an optimal switching policy, the General Pseudospectral Optimization Software (GPOPS) was used to solve the optimal control problem using an example trajectory.[14] A three-degree-of-freedom simulation was used in conjunction with relevant environment and vehicle models. Unless otherwise noted, the Mars atmosphere is modeled using Mars-GRAM.[15] Heat rate is calculated via the Sutton-Graves stagnation point convective heating equation.[16]

Fig. 4 shows two trajectories using an MSL baseline. Trajectory and vehicle parameters are provided in Table 1. Fig. 4 shows two trajectories: a full-lift-up trajectory with $u = L/D_{max}$ (the Viking strategy) and an optimal bang-bang trajectory, where u changes sign near 5 km/s (Fig. 4d). The optimal trajectory utilizes an initial lift-down command to dive into the atmosphere and quickly build dynamic pressure to increase lift later in the trajectory. Relative to the full-lift-up trajectory, the optimal trajectory decelerates at a lower altitude and exhibits only a small loft (Fig. 4a) and has a more shallow flight-path angle at the terminal condition (Fig. 4b). The improvement in terminal altitude is approximately 8.4 km, an improvement of nearly 40% relative to the lift-up trajectory. The cost of the improvement in terminal altitude is a significant increase in peak deceleration to nearly 7 g from 4.5 g (Fig. 4c).

Fig. 5 shows the Hamiltonian and costates for the optimal trajectory as functions of time. The Hamiltonian is small (Fig. 5a), and the co-states exhibit the expected behavior and satisfy the boundary conditions in Eq. (9) (Fig. 5b, c, d).

B. Validity of Optimal Control Solution

A region of validity in the entry state can be constructed for a given vehicle. To test the limits of the optimal control strategy, a vehicle was chosen with a high ballistic coefficient and low L/D. The properties shown in Table 2 were used to examine the entry state space. The entry velocity was swept from 5 to 8 km/s and the flight-path angle was swept from -5 to -20 deg. The results shown in Fig. 6 show the times of

Table 1. Example Trajectory Parameters

Parameter	Value
β	145 kg/m^2
L/D_{max}	0.24
V_0	5500 m/s
h_0	125 km
γ_0	-12 deg
V_f	1000 m/s
ρ_{ref}	0.02 kg/m^3
h_{ref}	0 km
H_{scale}	11100 m

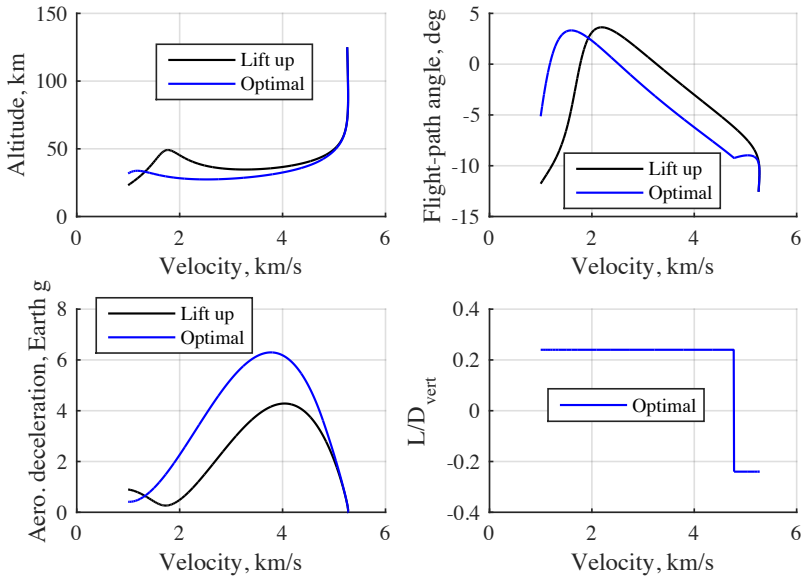

Figure 4. Example trajectory a) altitude, b) flight-path angle, c) deceleration, and d) vertical L/D as functions of relative velocity.

Table 2. Nominal vehicle and trajectory properties

Parameter	Value
β	450 kg/m^2
L/D_{max}	0.18
h_0	125 km
V_f	500 m/s
ρ_{ref}	0.02 kg/m^3
H_{scale}	11100 m

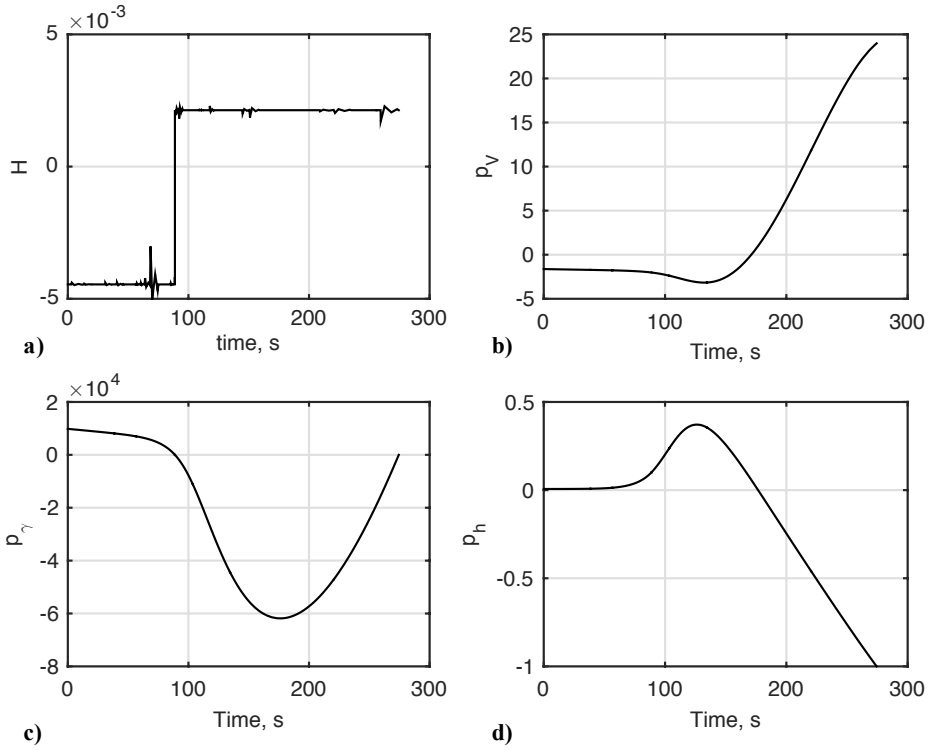

Figure 5. Example optimization parameters: a) Hamiltonian, b) velocity co-state, c) flight-path angle co-state, and d) density co-state as functions of time.

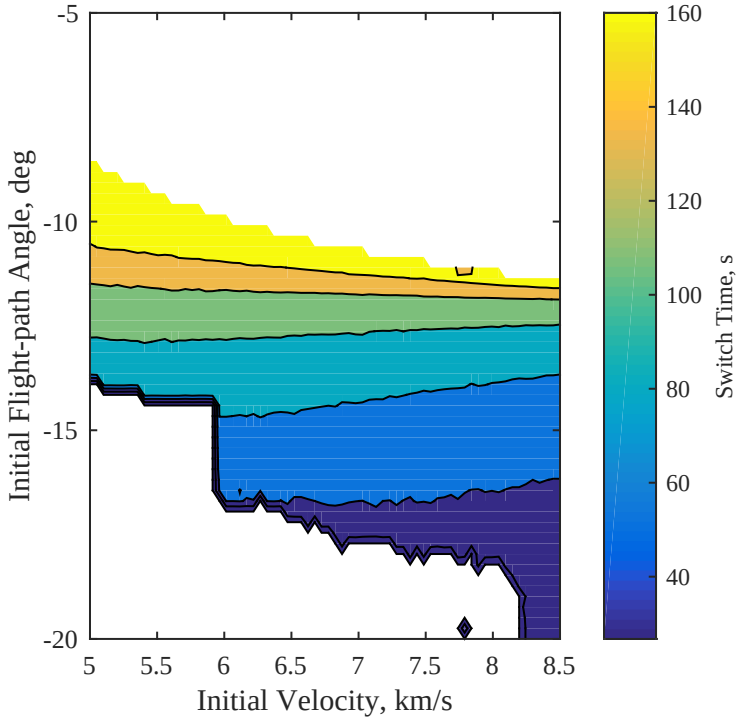

Figure 6. Contour of switch time for various entry states.

optimal switching for each state. The white region at the top represents trajectories which skip out of the atmosphere while the white region in the bottom represents trajectories with switch times at or near zero, i.e. the optimal bang-bang solution is equivalent to the full-lift-up solution.

A contour of final altitudes is shown in Fig. 7. The higher velocities tend to result in higher altitudes at terminal descent, though at the expense of an increase in loading and peak stagnation-point heat rate as seen on the right hand plot. Fig. 8 shows the difference in final altitude, peak deceleration, and peak heat rate using bang-bang optimal control versus a full lift up trajectory. Altitude gains of up to 4 km are possible at the cost of significant increases in peak deceleration and a minor increase in peak heat rate.

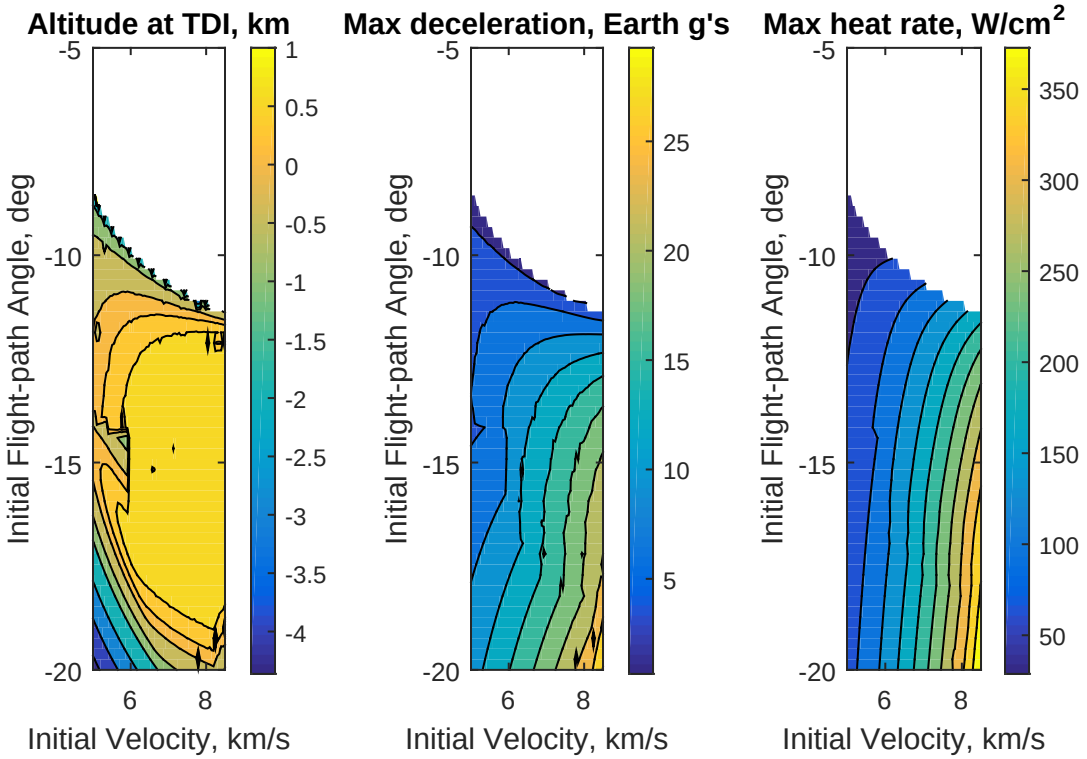

Figure 7. Contour of final landing altitude and maximum acceleration for various entry states.

III. Robustness of Optimal Control Solution

While the optimal switch point can be determined as a fixed time after entry interface, this is not likely a robust implementation in a flight system. Several different switching methods were tested via Monte-Carlo analysis in order to determine the most robust approach. Three parameters were used to determine robustness: flight path angle at terminal descent, landed altitude, and propellant mass used during terminal descent.

A. Setup

The trajectory parameters used in this study are shown in Table 3.

The Monte-Carlo dispersions correspond to pre-flight estimates for MSL (see Table 4)[17] and reduced by a factor of three to account for the lack of active guidance. Uncertainties in the atmospheric density vary as a function of altitude and are output in Mars-GRAM as 1-sigma variations. These were approximated with a quadratic function as shown in Fig. 9.

The descent stage is simulated with a simple "gravity turn" that uses full throttle with a constant thrust angle with respect to the horizon in order to bring the vehicle to zero velocity. No attempt was made to derive an optimal descent guidance strategy or incorporate pinpoint landing strategies. Rather, propulsive

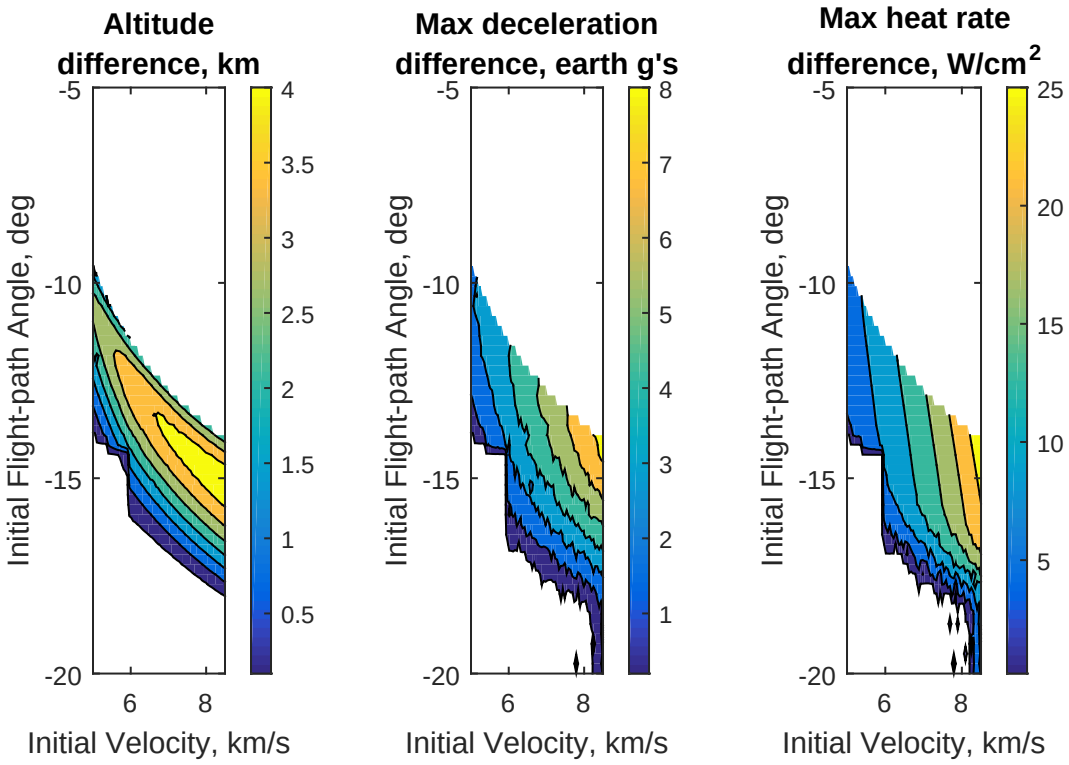

Figure 8. Gain in altitude and maximum acceleration for optimal control versus lift up.

Table 3. Monte-Carlo vehicle and trajectory properties

Parameter	Value
β	$\in 400 - 600$ kg/m^2
L/D_{max}	0.18
h_0	125 km
h_{TDI}	-2 km
Descent thrust	480,000 N
Engine I_{sp}	260 s

Table 4. Monte Carlo parameters and variations

Parameter	Nominal	Distribution	3-sigma
Entry flight-path angle	Variable	Gaussian	0.20 deg
Entry mass	Variable	Gaussian	2.0 kg
Drag force multiplier	1	Gaussian	3%
Lift force multiplier	1	Gaussian	8%

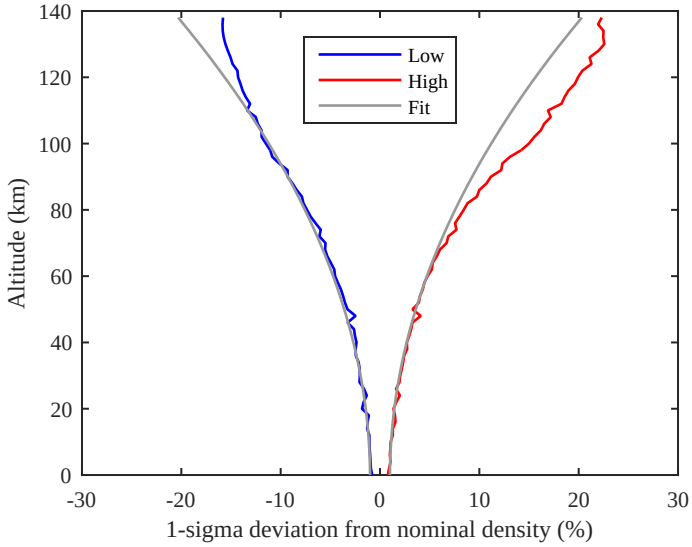

Figure 9. 1-Sigma Uncertainty in Atmospheric Density

descent is used to provide a high-level look at the control effort required to correct off-nominal trajectories. The equations of motion during this phase are shown in (10), (11), and (12) where u and v are the horizontal and vertical components of velocity, g is the gravitational acceleration, T is the total thrust, μ is the constant thrust angle (defined as zero facing forwards along the horizon), m_0 is the starting vehicle mass, g_0 is the gravitational acceleration on Earth, and I_{sp} is the propulsion system specific impulse.

$$\dot{u} = \frac{T}{m(t)} \cos \mu \tag{10}$$

$$\dot{v} = -g + \frac{T}{m(t)} \sin \mu \tag{11}$$

$$m(t) = m_0 - \frac{T}{g_0 I_{sp}} t \tag{12}$$

B. Trigger trends

The first bank reversal implementation analyzed was a simple time-based trigger. Assuming correct knowledge of the entry time, the bank reversal occurs after a set amount of time has passed, regardless of the vehicle state. The second trigger analyzed is velocity-based. Planet-relative velocity is a reliable piece of navigation knowledge, so using velocity to initiate the bank reversal could provide performance benefits over the time trigger. One interesting property of the optimal trajectories is that the optimal bank reversal velocity usually occurs near the peak dynamic pressure (q). However, this could be a result of the bank reversal itself rather than a natural outcome. To test this, the vehicle was plotted with both full lift-down and optimal velocity bank reversals. The results in Fig. 10 indicate that the optimal bank reversal point does indeed occur at or near the point of maximum dynamic pressure. Therefore, initiating a bank reversal at the point of max q could provide better robustness to dispersions than a time or velocity-based reversal.

A comparison between the time, velocity, and max q-based triggers is shown in Fig. 11. Results indicate that for a wide range of ballistic coefficients, the max q trigger is the most robust solution using the current metrics.

To test the applicability of the max q-based trigger, it is compared against the velocity trigger for a range of entry conditions. Fig. 12 shows a contour of the difference in final altitude between the two triggers. The max q trigger clearly performs poorly across a wide range of entry conditions, giving up as much as 5 km in altitude. This implies that for a wide range of cases the optimal switching time is not close to the time of maximum q. The difference is minimized around entry velocities of 8.5 km/s and flight path angles of

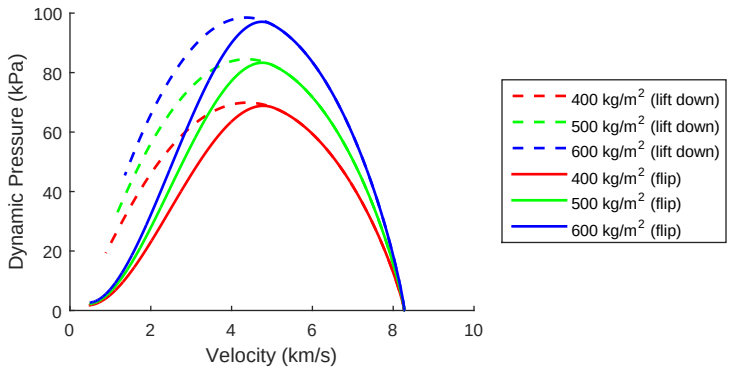

Figure 10. Region of maximum dynamic pressure for lift-down and optimal control

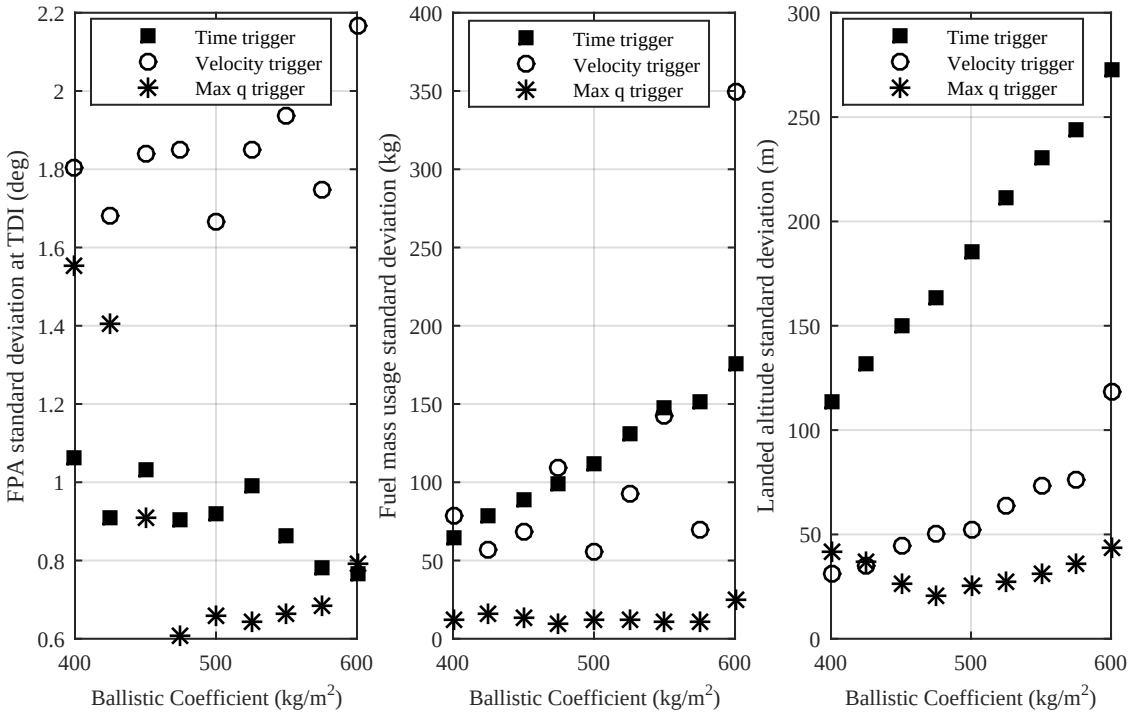

Figure 11. Comparison of robustness for time, velocity, and max q based reversal triggers

-12.5 degrees. Coincidentally, this is the region of maximum altitude for the velocity trigger (see Fig. 7). Therefore, for this design point (β = 450 kg/m^2, L/D = 0.18, V_0 = 8.5 km/s, γ_0 = -12.5 deg) the max q trigger offers altitude performance similar to that of the optimal velocity trigger.

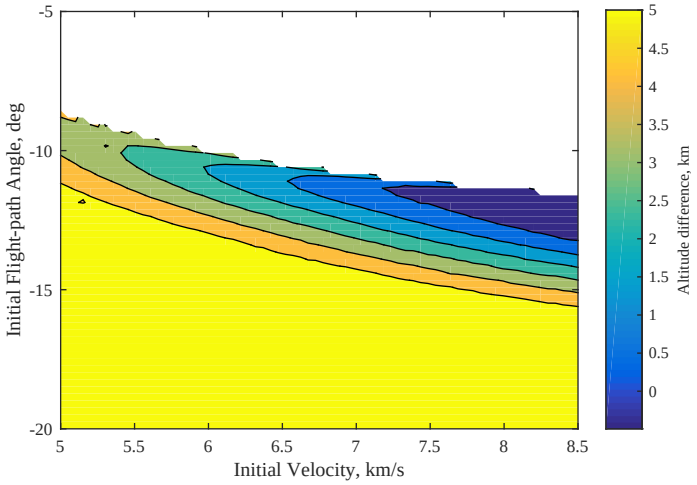

Figure 12. Altitude difference between velocity and max q triggers

C. Ancillary Effects of Optimal Control Solution

Flying lift-down for large portions of the trajectory, while providing good terminal altitude performance, has some significant drawbacks. These include deep dips that could potentially cause the vehicle to collide with high surface elevation terrain features, reduced timelines, and increased heating and deceleration.

1. Peak Deceleration

Since this flight strategy relies on the increase of dynamic pressure prior to the lift-up phase, sensed decelerations of ten to fifteen Earth g's may result for a case in which the full lift-up trajectory has a peak deceleration of approximately seven Earth g's. This may be acceptable for robotic missions but will require additional guidance constraints for human exploration. One method of reducing g-loading is to perform a shallow equilibrium glide at low velocities. By performing a bang-bang optimization while limiting the maximum flight path angle the vehicle is able to reach nearly the same terminal conditions with a decrease in peak sensed deceleration. This strategy forces a shallower descent rather than a deep dip followed by a loft. Results for a vehicle utilizing bang-bang lift control with various equilibrium glide angles are shown in Figs. 13 and 14. Input parameters are shown in Table 5. There is a one-to-one tradeoff between minimizing peak deceleration and maximizing final altitude. For given entry conditions, a mission designer could use this technique to find the equilibrium glide flight path angle that keeps the peak deceleration under the vehicle limit while maximizing altitude.

IV. Terminal Descent Initiation Triggers

Focus shifts now from bank reversal trigger analysis to terminal descent trigger analysis. Previous entry systems have relied heavily on velocity state, either directly or via dynamic pressure, to trigger parachute deployment.[18] However, when using SRP for terminal descent, velocity triggers do not appear robust in dispersed trajectories. Similarly, a pure altitude-based trigger (assuming altitude knowledge from a radar altimeter or some other sensor) may not be the optimal solution for reducing dispersions in propellant mass usage. A terminal descent trigger based on energy is investigated in this paper. The nondimensional energy $\bar{E}$ takes the form in Eq. (13). V_{ref} and h_{ref} are a velocity and altitude taken from the reference trajectory, h_{floor} is some minimum altitude, and $\lambda \in [0, 1]$ is a scaling factor between altitude and velocity. Note that

Table 5. Equilibrium glide test inputs

Parameter	Value
β	450 kg/m^2
L/D_{max}	0.18
h_0	125 km
V_0	7.5 km/s
γ_0	-13.5 deg
V_{TDI}	500 m/s

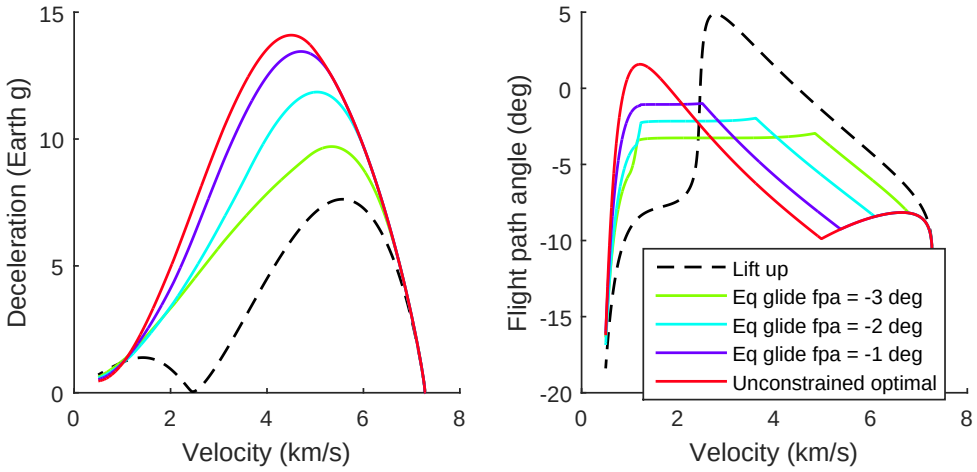

Figure 13. G loading and flight path angle for various equilibrium glide angles

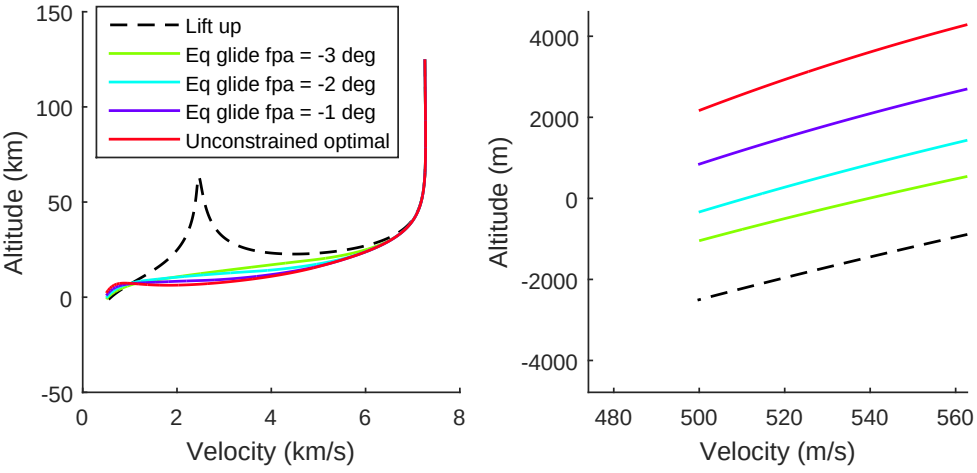

Figure 14. Altitude results with equilibrium glide

when $\lambda = 0$ the energy trigger reduces to a pure altitude based descent initiation trigger, and when $\lambda = 1$ it reduces to a velocity trigger.

$$\bar{E} = \lambda \frac{V^2}{V_{ref}^2} + (1 - \lambda) \frac{h - h_{floor}}{h_{ref} - h_{floor}} \tag{13}$$

The terminal descent phase begins once the vehicle energy falls below that set by the energy trigger (1 by default). The λ parameter can be varied to provide the best performance with respect to flight path angle, propellant mass, and landing altitude deviations as described above. Fig. 15 shown the results of using a dynamic pressure bank-reversal trigger with various energy trigger λ. The trigger is referenced to 700 m/s velocity and -250 m altitude.

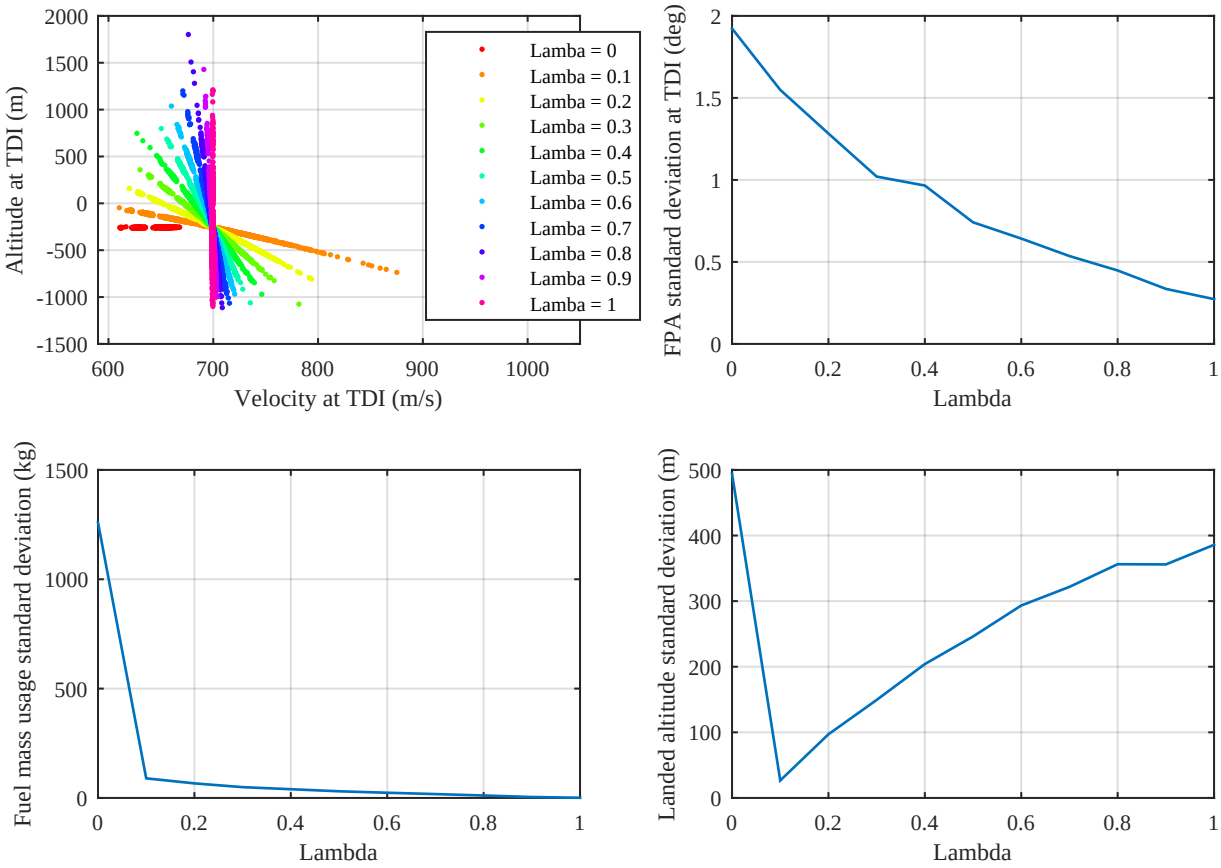

Figure 15. Monte Carlo results for various values of λ

Deviations in propellant mass and flight path angle decrease as the trigger approaches an altitude trigger; however, the pure altitude trigger ($\lambda = 0$) shows large deviations as certain cases reach the target altitude at speeds of up to 2.5 km/s. The landing altitude plot (bottom right) shows the opposite trend with altitude deviations increasing as the trigger approaches a velocity trigger. This result is intuitive as the spread in altitude at TDI increases with velocity triggers. These results suggest that the optimal TDI trigger depends largely on the specific guidance strategy used in terminal descent. For instance, high thrust systems may be able to absorb large altitude errors and will be best served with a high λ, while those with sufficient propellant margin may be better off with a low λ. Using energy to initiate terminal descent allows mission designers to gain the most benefit from this trade. Note these results do not take into account the ability of a vehicle to complete the required descent burn, which could be a driving design consideration for real missions.

V. Conclusions

Large ballistic coefficient vehicles are required to land larger masses and achieve more ambitious exploration goals at Mars. Requirements and guidance strategies for the use of aerodynamic lift in the hypersonic regime are assessed over a range of ballistic coefficients to provide sufficient timeline and altitude margin at terminal descent initiation. Results indicate that judicious use of lift may allow safe landing for a range of ballistic coefficients above current technology limits. A vehicle with $\beta = 450$ kg/m^2 and $L/D = 0.18$ can see altitude gains of 4 km while experiencing 8 g higher peak deceleration using a single bank reversal. Initiating this reversal upon max q rather than velocity or time can reduce the spread in flight path angle, propellant mass usage, and landing altitude during terminal descent. Large vehicles that utilize supersonic retropropulsion for descent cannot use a velocity trigger for descent initiation due to large possible variations in altitude. An energy trigger is proposed for better capturing the state of the vehicle, balancing altitude and velocity errors, and minimizing dispersions during terminal descent and landing.

References

[1]Braun, R. D. and Manning, R. M., "Mars Exploration Entry, Descent, and Landing Challenges," *Journal of Spacecraft and Rockets*, Vol. 44(2), March–April 2007, pp. 310–323.

[2]Hughes, Stephen J., Cheatwood, Dr. F McNeil, Dillman, Robert A., Wright, Henry S., DelCorso, Joseph A., "Hypersonic Inflatable Aerodynamics Decelerator (HIAD) Technology Development Overview," AIAA 2011-2524, May 2011.

[3]Clark, I. G., Adler, M., and Rivollini, T., "Development and Testing of a New Family of Supersonic Decelerators," AIAA 2013-1252, Mar. 2013.

[4]Korzun, A. M., Braun, R. D., and Cruz, J. R., "Survey of Supersonic Retropropulsion Technology for Mars Entry, Descent, and Landing," *Journal of Spacecraft and Rockets*, Vol. 46(5), Sep. 2009, pp. 929–937.

[5]McLellan, C. H. and Pritchard, E. B., "Use of Lift to Increase Payload of Unmanned Martian Landers," *Journal of Spacecraft and Rockets*, Vol. 3(9), Sep. 1966, pp. 1421–1425.

[6]Pritchard, E. B. and Harrison, E. F., "Lifting Entry ($L/D \leq 0.2$) for Unmanned Viking Class Mars Landers," NASA TN D-5828, Washington, DC, Jun. 1970.

[7]Braun, R.D., Powell, Richard W., Cheatwood, F. McNeil, Spencer, David A., and Mase, Robert A., "The Mars Surveyor 2001 Lander: A First Step Toward Precision Landing," 49th International Astronautical Congress, Melbourne, Australia, Paper IAF 98-Q.3.03, 1998

[8]Mendeck, G. F. and Craig, L. E., "Entry Guidance for the 2011 Mars Science Laboratory Mission," AIAA 2011-6639, Aug. 2011.

[9]Price, H.P.; Braun, R.D.; Manning, R.M.; and Sklyanski, E.; "A High-Heritage Blunt-Body Entry, Descent, and Landing Concept for Human Mars Exploration," Accepted for presentation at the 2016 AIAA Science and Technology Forum and Exposition, San Diego, CA, January 2016.

[10]Lafleur, J. M. and Cerimele, C. J., "Mars Entry Bank Profile Design for Terminal State Optimization," AIAA 2008-6213, Aug. 2008.

[11]Benito, J. and Mease, K. D., "Reachable and Controllable Sets for Planetary Entry and Landing," *Journal of Guidance, Navigation, and Control*, Vol. 33(3), May–June 2010, pp. 641–654.

[12]Garcia-Llama, E., "Apollo-Derived Terminal Control for Bank-Modulated Mars Entries with Altitude Maximization," AIAA 2008-6819, Aug. 2008.

[13]Vinh, N. X., Busemann, A., and Culp, R. D., *Hypersonic and Planetary Entry Flight Mechanics*, University of Michigan Press, Ann Arbor, MI, 1980.

[14]Rao, A. V., Benson, D. A., Darby, C. L., Patterson, M. A., Francolin, C., Sanders, I., and Huntington, G. T., "Algorithm 902: GPOPS, A MATLAB Software for Solving Multiple-Phase Optimal Control Problems Using the Gauss Pseudospectral Method," *ACM Transactions on Mathematical Software*, Vol. 37(2), Apr.Jun. 2010, Article 22.

[15]Justh, H. L. and Ramey, H. S., "Mars-GRAM 2010: Improving the Precision of Mars-GRAM," *4th International Workshop on the Mars Atmosphere: Modeling and Observations*, Feb. 2011.

[16]Sutton, K. and Graves, R. a., "A general stagnation-point convective heating equation for arbitrary gas mixture," NASA TR R-376, 1971.

[17]Striepe, S. A., Way, D., Dwyer, A., and Balaram, J., "Mars science laboratory simulations for entry, descent, and landing," *Journal of Spacecraft and Rockets*, Vol. 43, No. 2, 2006, pp. 311–323.

[18]Steltzner, A., Desai, P., Lee, W., and Bruno, R., "The Mars exploration rovers entry descent and landing and the use of aerodynamic decelerators", *17th AIAA Aerodynamic Decelerator Systems Technology Conference and Semi*